Modulation and Modeling of 3-Dimensional Nanowire Assemblies Targeting Gas Sensors with High Response and Reliability

*Hyeuk Jin Han, Gyu Rac Lee, Yujin Han, Hanhwi Jang, Eugene N. Cho, Sunho Kim, Chang Sub Kim, Soonmin Yim, Jae Won Jeong, Jong Min Kim, Seunghee Yu, Harry L. Tuller * and Yeon Sik Jung **

Dr. H. J. Han, G. R. Lee, Y. Han, H. Jang, Dr. E. N. Cho, Dr. S. Yim, Dr. J. W. Jeong, Dr. J. M. Kim, S. Yu, Prof. Y. S. Jung

Department of Materials Science and Engineering, Korea Advanced Institute of Science and Technology, 291 Daehak-ro, Yuseong-gu, Daejeon 34141, Republic of Korea

Dr. H. J. Han

Department of Mechanical Engineering and Materials Science, Yale University, New Haven, CT 06511, USA

Dr. S. Yim

Thin Film Materials Research Center, Korea Research Institute of Chemical Technology, Daejeon 34114, Republic of Korea

Dr. J. W. Jeong

Metal Powder Department, Korea Institute of Materials Science, Changwon 51508, Korea

Dr. J. M. Kim

Materials Architecturing Research Center, Korea Institute of Science and Technology, Seoul 02792, Republic of Korea.

This is the author manuscript accepted for publication and has undergone full peer review but has not been through the copyediting, typesetting, pagination and proofreading process, which may lead to differences between this version and the Version of Record. Please cite this article as doi: 10.1002/adfm.202108891.

Dr. S. Kim, Dr. C. S. Kim, Prof. H. L. Tuller

Department of Materials Science and Engineering, Massachusetts Institute of Technology, Cambridge, Massachusetts 02139, USA

E-mail: tuller@mit.edu, ysjung@kaist.ac.kr

Keywords: nanoarchitecture, metal oxides, gas sensors, nano-transfer printing

Despite improved sensitivity, simple downsizing of gas-sensing components to randomly arranged nanostructures often face challenges associated with unpredictable electrical conduction pathways. In the present study, we demonstrate controlled fabrication of three-dimensional (3D) metal oxide nanowire networks that can greatly improve both signal stability and sensor response compared to random nanowire arrays. For example, the highest ever reported H_2S gas response value, and 5 times lower relative standard deviation of baseline resistance than that of random nanowires assemblies, were achieved with the ordered 3D nanowire network. Systematic engineering of 3D geometries and their modeling, utilizing equivalent circuit components, provided additional insights into the electrical conduction and gas-sensing response of 3D assemblies, revealing the critical importance of wire-to-wire junction points and their arrangement. These findings suggest new design rules for both enhanced performance and reliability of chemical sensors, which may also be extended to other devices based on nanoscale building blocks.

1. Introduction

Over the past decades, chemical sensors based on nanoscale-engineered metal oxide semiconductors (MOS) have demonstrated the capability of detecting a wide range of gas species

with high sensitivity. Key factors in achieving improved performance include high surface-to-volume ratios, high surface activities, and the use of a variety of material candidates for gas selectivity. For example, significant increases in sensitivity can be achieved by full depletion and accumulation of carriers in sensing channels. This effect can be realized in sensing materials with grain sizes of less than ~10 nm[1,2], as well as at grain boundaries and sintered necks, dominated by space charge barriers. In order to reflect these design factors, various fabrication techniques have been developed, leading, in turn, to a variety of nano-building blocks including nanotubes, nanoribbons, nanowires, nanoparticles, and hollow spheres suitable for gas sensing.[3–5]

Although significant advances have been made in MOS-based gas sensors through nano-engineering, integrating MOS nanostructures into gas sensors is not trivial as nano-engineering does not always benefit gas sensor properties.[6] For example, sensitivity increases substantially with decreasing grain size,[2,6,7] however, the effective electrical conductivity can be drastically reduced due to increases in both interfacial space charge barriers and the density of grain boundaries.[6] Since the reduced electrical conductivity requires more sophisticated measurement circuits,[6,8] conventional nanostructures for gas sensors have been fabricated by increasing packing density or loading level to reduce sensor resistance. Theoretically, if the same nano-building blocks are parallel connected, the resistance will be diminished, proportional to the number of connected components, while retaining the same sensitivity. However, the electrical properties and gas response often depend on packing density and loading level, which commonly shows a lower sensitivity with reduced resistance even though the gas sensor consists of nominally near identical nano-structured elements.[4,6]

Moreover, given the morphological complexity of typical assemblies of MOS nanostructures, along with uneven distribution of nano-building block agglomeration, a quantitative analysis of the intrinsic contributions of nano-building blocks, and the effect of structure on sensor performance, is a formidable challenge. Thus, even though some reports discuss the effects of structure at all levels, on sensitivity,[9,10] the underlying question of the exact role of nano-building blocks on the electrochemical reactions, and therefore performance, remains unclear. To enhance understanding, aid optimization, and provide guidance for future applications, a more systematic strategy is needed to extrapolate details from individual nano-building blocks to the properties of macroscopic assemblies.

To address these issues, we report a gas sensor with cross-stacked 3-dimensional (3D) MOS nanostructures, fabricated by nanotransfer printing, which allows for the creation of reproducible nano-building blocks and their assembly into controlled 3D nanostructures. The highly ordered and systemically controlled nanostructures are highly useful to provide models for investigating the role of 3D features on conduction in such assemblies of nano building blocks and how to optimize sensor performance. Combining models and experimental results, we confirm the 3D-assembled MOS nanostructures can serve to simultaneously improve signal stability, enhance conductance, and response, based on dense and regular zero-dimensional contact points between nanowires. Moreover, the reported fabrication flexibility should enable the extension of these processes to a diverse range of metal oxide materials, including catalysts decorated nanostructures with high sensitivity and selectivity. Pt-decorated n-type SnO_2 nanowire based 3D nanostructures examined in this study, for example, achieve a high response value of 1285.8 (at 1 ppm H_2S) that is 3.7 times higher than that of the state-of-the-art H_2S gas sensor.[11]

2. Results

2.1. Fabrication of 3D nanowire assemblies via printing of nanoscale building blocks

The key requirement to achieving a 3D-ordered MOS nanoarchitecture is the fabrication capability to align nanowire arrays and transfer these arrays sequentially onto substrates. The schematic in Figure 1a shows that high-yield (nearly 100%) direct transfer of nanostructures onto receiver substrates can be realized by solvent-assisted nanotransfer printing (S-nTP), based on an adhesion switching mechanism developed by our group.[12,13] Through sequential printing of the nanowire arrays, multi-stacked 3D crossed-wire nanostructures are capable of being fabricated with controlled numbers of stacking layers. Figure 1b-i shows a scanning electron microscopy (SEM) image of a highly ordered 2D periodic nanowire array made up of 50-nm-wide lines spaced 50 nm apart and formed over a large area (2 cm × 2 cm), as represented in the inset image. A highly porous multi-stacked 3D crossed-wire MOS nanostructure composed of SnO_2 is shown in both top-down and tilt-view SEM images in Figure 1b-ii. These highly ordered nanostructures are compared with disordered SnO_2 nanostructures (drop-casted nanowires and screen-printed nanoparticles as shown in the SEM images (Figure 1c-i and Figure 1c-ii). To crystallize the SnO_2 and achieve structural stabilization, the fabricated MOS nanostructures were then annealed at temperatures of 500 °C in the air for 6 h.

The crystallization of the printed nanowires was confirmed by transmission electron microscopy (TEM) images, which showed small grains with an average grain size of ~ 5.5 nm (Supplementary

Figure S1, see references for details).[14] The high-resolution transmission electron microscopy (HRTEM) image of SnO_2 nanowires with selected area electron diffraction (SAED) pattern clearly shows the SnO_2 (110) plane (lattice fringe spacing = 0.33 nm) while the respective energy dispersive X-Ray (EDX) analysis shows the presence of Sn and O (Supplementary Figure S2a-c).

Moreover, it is conventionally challenging to fabricate the same structure composed of different materials. However, the method described in this study can produce essentially geometrically identical nanoscale building blocks from different source materials (e.g., NiO, p-type MOS). The HRTEM image of NiO nanowires with SAED pattern clearly shows the NiO (111) plane (lattice fringe spacing = 0.24 nm) while the respective EDX analysis shows the presence of Ni and O (Supplementary Figure S2d-f).

The SEM images of the nanowire arrays and 3D nanoarchitecture obtained from nano-transfer printing (Figure 1b) reveal several important features. First, the printed nanowires achieved excellent alignment without breaks over their full lengths which would be important to obtain reproducible electronic properties, as well as uniform inter-wire spacing (see details in the Supplementary Discussion S3). As demonstrated in Figure 1b-i, extremely straight and parallel nanowires were obtained regardless of position within the arrays. Quantitative analysis on more than 100 nanowires (Figure 1d) shows that ~97.0% of the transfer-printed nanowire are aligned within an angle of ±1°. Transfer-printing can thus assure outstanding reproducibility in device performance, essential for commercialization, although this aspect is often not discussed in the literature. In this study, in order to characterize the reproducibility and regularity of measured electrical data, the relative resistance (resistance/average resistance) of sensors was measured and depicted in the histogram obtained from 40 sensors (Figure 1e). The 2D nanowire array with a relative standard deviation (RSD) of 3.70% and 2-layer crossed nanowires with an RSD of 2.11%

demonstrated considerably better device-to-device reproducibility than drop-casted nanowires (RSD of 59.70%) and screen-printed nanoparticles (RSD of 49.03%).

2.2. Engineering 3D structures and materials for maximizing sensor performances

For high sensitivity, nanostructures in chemiresistor sensors should be engineered so that nano-dimensioned building blocks are nearly or fully depleted of free carriers, which inevitably results in excessively high electrical resistances.[6,7] The resistance of sensors, however, can be reduced by achieving multiple parallel connections between nano-building blocks. However, without systematic nano-engineering, three-dimensional nanostructures are typically highly disordered with unpredictable and non-uniform junctions between nano-building blocks. This lack of structural controllability leads inevitably to reliability and reproducibility issues. Furthermore, due to the random aggregation of nano-building blocks, sensitivity is reduced. In order to resolve this challenge, we designed 3D cross-stacked nanowire arrays, that are comprised of massive parallel resistor connections, while retaining high sensitivity by preventing the agglomeration of nano-building blocks. This unique structure provides high surface-to-volume ratios and narrow wire-to-wire contact points for enhanced sensitivity and parallel electrical pathways for low electrical resistance, while ensuring well-defined empty channels between the nanowires for facile gas penetration as illustrated in Supplementary Figure S3.

To elucidate the influence of structure in printed SnO_2 nanowires on gas-sensing performance, we characterized the response of the 3D nano-architectured devices with various numbers (L; 1, 2, 3, 4, and 8) of nanowire stacking layers. The base line resistance of the samples in air was observed to

decrease with increasing L. For example, an almost 28-fold reduction in resistance (at 350 °C in air atmosphere) was achieved by increasing L from 1 (700 kΩ) to 8 (27.1 kΩ) (Figure 2a). Figure 2b presents the dynamic ethanol sensing response ($S = R_{air}/R_{gas}$, where R_{air} and R_{gas} are the resistances of the sensor in air and analytic gas, respectively) for different structures (thin film, L = 1, 2, 4 and 8 layers) of SnO_2, as the concentration of ethanol decreased from 100 to 5 ppm at 350 °C. The 2D nanowire arrays (L = 1) and 3D nanoarchitecture (L = 2) exhibited 13.2 and 23.8 times higher response than the SnO_2 thin film sensor, respectively, because of higher surface-to-volume ratios compared to the reference thin film counterpart.

Interestingly, in contrast to conventional sensor platforms, where there is commonly a trade-off between the magnitude of the resistance and response (Supplementary Figure S4),[4,6,15] cross-stacked nanowire structures show an opposite trend – increasing response with decreasing baseline resistance as L goes up (Figure 2a and 2c). For the same concentration of molecules, the 2-layer-stacked sample showed almost 2 times higher response than the mono-layered nanowire array structure (Figure 2c). For example, the response at 100 ppm ethanol (red circle in Figure 2c), the 2-layered (33.7), 3-layered (34.7), 4-layered (35.1) and 8-layered (34.2) samples were nearly 2 times higher than the single-layer nanowire array (16.4). Also, there is a similar enhancement trend found upon exposure to other target gases such as benzene (blue triangle in Figure 2c) and toluene (green square in Figure 2c).

Analogous to the SnO_2 nanostructures, a similar nanowire array, but this time composed of p-type NiO nanostructures, exhibited a considerably higher response (11.0 times) than a 20 nm NiO thin film reference, as well as more rapid response and shorter recovery times (Supplementary Figure S5). Relative to the film, the enhancement factor of the response (R_{gas}/R_{air}) for the NiO stacked structure

was approximately 28.2. This demonstrates the general versatility of the application of highly organized 3D nanoarchitecture to, in principle, an unlimited number of different materials systems.

Furthermore, while response time, defined as the time to reach 90% variation in resistance upon exposure to target gases, usually goes up with increasing loading amount and packing density, the multi-stacked nanostructure (22 sec), 6.5 times faster than the thin film structure (20 nm), showed a similar response time to that of the 2D nanowire arrays (24 sec) even as the loading amount increases 8 fold, without loss of sensitivity (Figure 2d). This can be attributed to the structural advantages that provide large channels for facile gas infiltration, without loss of sensitivity.

Metal oxide gas sensors, operated at elevated temperatures (i.e. 300 – 400 °C), tend to exhibit long-term thermal instability as reflected in response sensitivity changes, signal drift and ultimately failure.[16,17] The fabricated ordered 3D network structure in this study, on the other hand, shows longer-term thermal stability compared to 2D nanowire arrays (L=1), in concert with previous reports that network structures show more robust performance[18]. Figure 2e shows the resistance changes for the stacking layers examined (L= 1, 2, 4, and 8) for up to 120 h at 350 °C. The baseline resistance was measured as a function of time. Initially, the sensor resistance rose rapidly within the first 10 hours, including the initial burn-in time. The resistance of the nanowire array increased from the initial value by a factor of 1.98, while the stacked structure (L=4) increased only by a factor of 1.21. With respect to gas response, the stacked structure (L=2, 4, 8) exhibited a 2.02 times higher response than the nanowire arrays (L=1), as demonstrated in Figure 2f. After 120 h of operation at 350 °C, the change of gas response from the initial value ($\Delta S/S_0$, where $\Delta S = S_{max}-S_0$) was within 10.1% for the stacked structure (L=8), while it was 22.3% for the nanowire arrays. These results confirm that the 3D nano-architecture-based sensor exhibit improved long-term stability.

To further demonstrate the versatility of our fabrication technique in providing additional functionality,[19] we describe how catalytic elements can be incorporated onto the 3D nanoarchitectures. For example, in the following, we describe Pt-incorporated SnO_2 nanowire assemblies (Supplementary Figure S6a). SnO_2 and Pt were sequentially deposited onto our PMMA replica as a layered-nanowire structure to achieve Pt decoration onto the surfaces of the SnO_2 nanowires. Figure 3a shows high-angle annular dark-field scanning TEM image and EDX mapping of the Pt decorated SnO_2 nanowires. These clearly exhibit the contributions of Pt, Sn and O and reveal that the SnO_2 nanowire shells were uniformly decorated with Pt particles. Lattice distances of the (110) plane of SnO_2, (0.34 nm) and the (111) plane of Pt (0.23 nm) are clearly shown in the HRTEM image (Supplementary Figure S6b). We also analyzed the SAED pattern (Fig. S6c) and EDX spectra (Fig. S6d) of the Pt decorated SnO_2 nanoribbons, which show the uniform formation of Pt on the SnO_2NWs. The Pt decorated SnO_2 nanowire structures were tested to investigate the impact of Pt decoration on sensor response. Figure 3b compares the gas sensing responses of undecorated SnO_2 and Pt-decorated SnO_2 stacked nanostructures upon exposure to 1−4 ppm of ethanol at 350 °C. At 1 ppm ethanol exposure, the 6 nm Pt-decorated SnO_2 nanowire showed substantially enhanced performance (S= 12.16, response time: 14 s at 1 ppm), a 4.5 times higher response and 60% shorter response time than that of the Pt free SnO_2 structure (S = 2.70). Interestingly, in the case of the Pt (6 nm)/SnO_2 nanowire annealed at 700 °C in air, a colossal enhancement in hydrogen sulfide response (S = 1285.8 at 1 ppm) at 300 °C was observed compared to that of the undecorated SnO_2 nanowires (S = 11.1 at 1 ppm.) (Figure 3c). This is one of the highest hydrogen sulfide response values ever reported in the literature (Figure 3d and Supplementary Table S1).[11,20–28] In addition, the Pt (6 nm)/SnO_2 nanowires were strongly selective to hydrogen sulfide with only minimal response towards other interfering gases under 1 ppm (Supplementary Figure S7).

2.3. Electrical characterization of 3D assemblies

To investigate the electrochemical response of the structurally defined MOS sensor nanostructures, we examined the response by impedance spectroscopy. Data obtained for several different nanostructures following exposure to CO in the concentration range of 100–1000 ppm at 350 °C, are depicted in the form of Nyquist plots, and the equivalent electrical circuits of the nanowire arrays and the stacked nanostructures are shown in Figure 4a and 4b, respectively. The spectra for the nanowire arrays are fit to a circuit consisting of an offset resistance in series with a single RC semicircle centered at ~80 Hz when measured in air as shown in Figure 4a. The stacked nanostructures are fit to a slightly more complex circuit composed of an offset resistance in series with two RC semicircles centered at ~100 Hz and ~2000 Hz, respectively, as shown in Figure 4b. By comparing the results in Figure 4a and 4b, it becomes clear that the additional high-frequency (~2000 Hz) contribution in the stacked nanostructures derives from the contact points between the nanowires in adjacent layers that do not exist in the simple nanowire array. The common RC contribution characterized by the lower frequency contribution centered at ~100 Hz must reflect the characteristics of the electrochemical reactions occurring on the surfaces of the nanowire body. In brief, we assign the characteristic electrical component of the nanowire array to R_{wire}, while the 3D nanoarchitecture exhibits an additional electrical circuit component, the sum of which we assign to $R_{wire} + R_{junction}$ where $R_{junction}$ reflects the contribution due to the contact points between nanowires in adjacent layers.

The relative response of each component (R_{wire} and $R_{junction}$) was then examined as a function of CO concentration (Figure 4c). For the one-layer nanowires, modeled with a single resistor component (R_{wire}^{1L}), the slope of the response to CO gas concentration was 0.69/dec. In the case of the two-layer stacked nanostructure, the resistance of the two components (R_{wire}^{2L} and $R_{junction}^{2L}$), calculated from impedance spectroscopy, show different slopes of 0.71/dec and 1.38/dec, respectively. These results demonstrate that R_{wire} shows a similar sensitivity regardless of whether stacking layers exist or not, but that $R_{junction}$ exhibits a higher sensitivity than R_{wire}, consistent with our observation of the enhanced response of our stacked vs single layer nanostructures. In addition, the effect of $R_{junction}$ on the response could also be confirmed through network structures containing artificial cracks, which increases the contribution of $R_{junction}/R_{wire}$ in the circuit (see more details in the Supplementary Discussion 1) by forcing current flow through the junction points.

In order to provide a more quantitative analysis of the sensor performance of our network structures, electrical conduction through the nanowires, can be represented by an elementary resistor network as shown in Figure 4d (see detailed circuit analysis in the Supplementary Discussion 2). Based on these analyses, the calculated relative response (S_L/S_1, see more details in the Supplementary Discussion 4), defined as the ratio ($S = R_{eq,air}/R_{eq,gas}$), are predicted to show a dependence on stacking layer number as shown in Figure 4e (black squares). These predictions match well with the experimental response (Figure 4e, red circles) that shows increased response with increasing stacking layer number, confirming our initial hypothesis that 3D stacking can contribute to improved gas response by forming contact points (see detailed in the Supplementary Discussion 4). Even though there was less significant enhancement in response for the number of stacked layers higher than 2, stacking more layers also improved conductance and long-term

stability with maintaining a similar response time, which will be more advantageous for practical use and commercialization.

3. Conclusion

In summary, we have demonstrated the ability to prepare large area, highly aligned and uniform metal oxide nanowire arrays and stacked 3D crossed-wire nanostructures *via* solvent-assisted nanotransfer printing. These ordered structures show excellent alignment and regularity and a considerably lower standard deviation of resistance (~5.28%), 5 times lower than that achieved from disordered structures. Our measurements demonstrated that 3D nanowire assemblies exhibit superior gas response, decreased equivalent resistance in air and improved signal stability compared to thin films or 3D array counterparts. By combining electrical characterization with equivalent circuit modeling, the role of 3D nanostructure in influencing sensor performance was elucidated. These results suggest more advanced design rules for high performance sensors, e.g. by demonstrating the significantly enhanced sensitivity provided by forming contact points between adjacent layers of nanowire building blocks. Moreover, the presented fabrication method is broadly applicable to a diverse range of oxide materials and catalysts used to decorate them. Hybrid 3D nanostructures based on Pt decorated SnO_2 achieved a colossal response value of 1285.8 (at 1 ppm H_2S) relative to a reference film and 3.7 times higher than that of the state-of-the-art H_2S gas sensor. An improved understanding of the role of nanostructure in influencing sensor performance correspondingly aids in developing improved design rules for high performance sensors, and the flexibility of fabrication points to the ability to extend these processes to diverse applications

including multifunctional sensors and catalysts, and with additional modifications to batteries, fuel cells and other functional devices.

4. Experimental Section

Silicon Master Mold Preparation: Si master molds were fabricated using KrF photolithography followed by reactive ion etching. A positive photoresist (PR, Dongjin Semichem Co. Ltd.) with a thickness of 1 μm was spin-coated onto 8 in. Si wafers. The PR was then exposed using a KrF scanner (Nikon, NRS-S203B), followed by developing using a developer solution (tetramethyl ammonium hydroxide, Dongjin Semichem Co. Ltd.) The PR patterns were used as an etch mask to pattern the Si wafer surface by reactive ion etching (gas, CF_4 for etching, C_4F_8 for wall passivation; working pressure, 10 mTorr; plasma power, 165 W).

Fabrication of the Metal Oxide Nanowire Array and 3D Nanoarchitecture: Prior to replication, the surface of the master mold was treated with a PDMS brush (Polymer Source Inc.). PMMA (M.W. = 100 kg mol^{-1}) purchased from Sigma-Aldrich Inc. and was dissolved in a mixed solvent of toluene, acetone, and heptane (4.5:4.5:1 by volume) to yield 4 wt% solutions. The solution was spin-cast onto the master mold with a spin speed of 4000 rpm. A polyimide adhesive film (3M Inc.) was then attached onto the surface of the polymer replica. By removing the adhesive film from the mold, the replica with an inverted image of the surface topography of the master mold was detached from the mold. Nanowires were formed through 20 nm deposition of target materials (SnO_2, NiO) onto the polymer replica using a e-beam evaporator. The deposition angle from the substrate surface normal

was modulated and optimized at 80°. Acetone/heptane vapor was applied to the polymer replica film by placing the replica/adhesive film into a solvent saturated chamber that was preheated to 55 °C. After 20 s, the adhesive film was removed from the chamber and brought into contact with the Si substrates with a 300 nm thick SiO_2 layer. Mild pressure was applied for uniform contact between the nanowire/replica/adhesive film and the substrate. The adhesive film was selectively detached from the substrate while the nanostructure/replica remained on the receiver substrate. Uniformly arranged nanowires on the substrate could then be obtained by washing away the polymer replica film using toluene. After the first layer of the metal oxide nanowire arrays is transferred, the second layer is printed on top of the first layer with an alignment angle of 90° for 3D nanoarchitecture fabrication.

Characterization of Materials: For characterization of the samples, a field emission SEM (Hitachi S-4800) was used with an acceleration voltage of 10 kV, and a working distance of 5 mm. HRTEM images and EDS mapping were obtained using a 200 kV accelerating voltage TEM (FEI, Talos F200X). To prepare the samples used in TEM, the nanostructures on Si substrates with 300 nm thick SiO_2 surface layers were detached by HF treatment and transferred onto a Cu TEM grid.

Gas Sensor Fabrication and Gas Delivery System: The fabricated nanostructures were annealed at 500 °C in air for 6 h for stabilization. To measure the resistance signal, two electrodes were fabricated using conventional photolithography. Photoresist (AZ-5214E) was spin-cast onto the metal oxide nanostructure /SiO_2/Si substrate and electrode regions were defined with 20 μm spacings (MDA-8000B). After development of the photoresist, Ni (10 nm) / Au (100 nm) electrodes were deposited by e-beam evaporation, followed by lift-off with acetone. The resulting two-probe resistor-type sensors were mounted within a sensing chamber fabricated in-house. The sealed gas

sensing chamber, with dimensions of approximately 5 cm in diameter and 20 cm in length, were inserted into a tube furnace within which the gas sensors were heated to 350 °C. A gas delivery system, built in-house, was used to control the gas flow into the sensing chamber to measure the sensor response at ambient pressure. Dry air was used as the reference gas, and the total flow rate was fixed at 500 cc/min.

Electrical Measurements: The resistance of the sensing channels was recorded in real time using a data acquisition module (34970A; Agilent Technologies) under constant flow and temperature in a tube furnace. The impedance spectra were measured with a potentiostat/impedance analyzer (Solartron Analytical, ModuLab XM MTS) utilizing low-amplitude sinusoidal voltages (50 mV) in the frequency range of 10^{-3} to 2 MHz and fitted with the aid of Zview Software (Scribner Associates).

Supporting Information

Supporting Information is available from the Wiley Online Library or from the author.

Acknowledgements

This work was supported by the National Research Foundation of Korea (NRF) grant funded by the Ministry of Science and ICT (NRF-2019R1A2C2086240). HL Tuller thanks the U.S. Department of Energy (DOE), Office of Science, Basic Energy Sciences (BES) under Award # DE-SC0002633 for his support.

Conflict of Interest

The authors declare no conflict of interest

Received: ((will be filled in by the editorial staff))
Revised: ((will be filled in by the editorial staff))
Published online: ((will be filled in by the editorial staff))

References

[1] S. Y. Cho, H. W. Yoo, J. Y. Kim, W. Bin Jung, M. L. Jin, J. S. Kim, H. J. Jeon, H. T. Jung, *Nano Lett.* **2016**, *16*, 4508.

[2] N. Barsan, U. Weimar, *J. Electroceramics* **2001**, *7*, 143.

[3] M. Mehdi Pour, A. Lashkov, A. Radocea, X. Liu, T. Sun, A. Lipatov, R. A. Korlacki, M. Shekhirev, N. R. Aluru, J. W. Lyding, V. Sysoev, A. Sinitskii, *Nat. Commun.* **2017**, *8*.

[4] J. Shin, S. Choi, I. Lee, D. Youn, C. O. Park, J. Lee, H. L. Tuller, I. Kim, *Adv. Funct. Mater.* **2013**, *23*, 2357.

[5] N. G. Cho, G. C. Whitfield, D. J. Yang, H. G. Kim, H. L. Tuller, I. D. Kim, *J. Electrochem. Soc.* **2010**, *157*.

[6] A. Tricoli, S. E. Pratsinis, *Nat. Nanotechnol.* **2010**, *5*, 54.

[7] N. Barsan, M. Schweizer-Berberich, W. Göpel, *Fundamental and practical aspects in the design of nanoscaled SnO2 gas sensors: A status report*, **1999**.

[8] J. Yao, H. Yan, C. M. Lieber, *Nat. Nanotechnol.* **2013**, *8*, 329.

[9] R. Khan, H. W. Ra, J. T. Kim, W. S. Jang, D. Sharma, Y. H. Im, *Sensors Actuators, B Chem.* **2010**, *150*, 389.

[10] S. Phadke, J. Y. Lee, J. West, P. Peumans, A. Salleo, *Adv. Funct. Mater.* **2011**, *21*, 4691.

[11] S. Kim, S. Choi, J. Jang, H. Cho, W. Koo, H. L. Tuller, I. Kim, *Adv. Mater.* **2017**, *29*, 1700737.

[12] J. W. Jeong, S. R. Yang, Y. H. Hur, S. W. Kim, K. M. Baek, S. Yim, H. I. Jang, J. H. Park, S. Y. Lee, C. O. Park, Y. S. Jung, *Nat. Commun.* **2014**, *5*.

[13] H. J. Han, J. W. Jeong, S. R. Yang, C. Kim, H. G. Yoo, J.-B. Yoon, J. H. Park, K. J. Lee, T.-S. Kim, S.-W. Kim, Y. S. Jung, *ACS Nano* **2017**, *11*, 11642.

[14] H. J. Han, G. R. Lee, Y. Xie, H. Jang, D. J. Hynek, E. N. Cho, Y. J. Kim, Y. S. Jung, J. J. Cha, *Sci. Adv.* **2021**, *7*, eabh2012.

[15] S. W. Lee, P. P. Tsai, H. Chen, *Sensors Actuators, B Chem.* **2000**.

[16] T. Waitz, T. Wagner, T. Sauerwald, C. Kohl, M. Tiemann, *Adv. Funct. Mater.* **2009**, *19*, 653.

[17] R. C. Singh, M. P. Singh, O. Singh, P. S. Chandi, *Sensors Actuators, B Chem.* **2009**, *143*, 226.

[18] G. Pennelli, M. Totaro, M. Piotto, P. Bruschi, *Nano Lett.* **2013**, *13*, 2592.

[19] H. J. Han, S. H. Cho, S. Han, J. Jang, G. R. Lee, E. N. Cho, S. Kim, I. Kim, M. S. Jang, H. L. Tuller, J. J. Cha, Y. S. Jung, *Adv. Mater.* **2021**, 2105199.

[20] S. J. Kim, S. J. Choi, J. S. Jang, N. H. Kim, M. Hakim, H. L. Tuller, I. D. Kim, *ACS Nano* **2016**, *10*,

5891.

[21] T. Yang, Q. Yang, Y. Xiao, P. Sun, Z. Wang, Y. Gao, J. Ma, Y. Sun, G. Lu, *Sensors Actuators, B Chem.* **2016**, *228*, 529.

[22] J. S. Jang, S. J. Kim, S. J. Choi, N. H. Kim, M. Hakim, A. Rothschild, I. D. Kim, *Nanoscale* **2015**, *7*, 16417.

[23] J. Shi, Z. Cheng, L. Gao, Y. Zhang, J. Xu, H. Zhao, *Sensors Actuators, B Chem.* **2016**, *230*, 736.

[24] J. Shin, S. J. Choi, D. Y. Youn, I. D. Kim, *J. Electroceramics* **2012**, *29*, 106.

[25] S. J. Choi, B. H. Jang, S. J. Lee, B. K. Min, A. Rothschild, I. D. Kim, *ACS Appl. Mater. Interfaces* **2014**, *6*, 2588.

[26] F. E. Annanouch, Z. Haddi, S. Vallejos, P. Umek, P. Guttmann, C. Bittencourt, E. Llobet, *ACS Appl. Mater. Interfaces* **2015**, *7*, 6842.

[27] Y. L. Liu, Z. M. Liu, Y. Yang, H. F. Yang, G. L. Shen, R. Q. Yu, *Sensors Actuators, B Chem.* **2005**, *107*, 600.

[28] T. Yu, X. Cheng, X. Zhang, L. Sui, Y. Xu, S. Gao, H. Zhao, L. Huo, *J. Mater. Chem. A* **2015**, *3*, 11991.

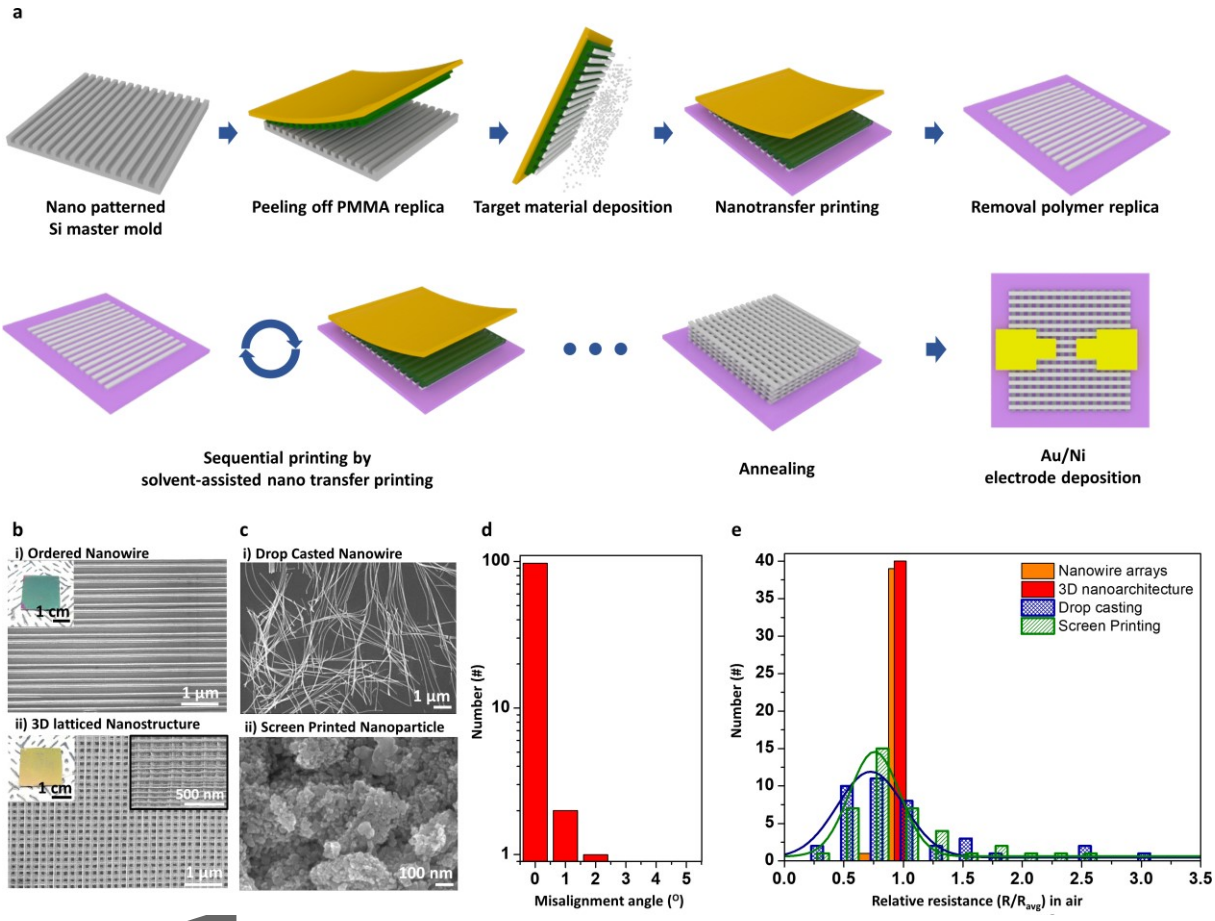

Figure 1. Schematics and demonstration of 3D nanowire array fabrication. a. Schematics of the nanowire array fabrication process via nano-transfer printing (see Methods for details). **b.** SEM images of ordered nanostructures i) printed nanowire array ii) multi-stacked 3D nanoarchitecture **c.** SEM images of disordered nanostructure i) drop-cast nanowires ii) screen-printed nanoparticles **d**, Angular distribution of printed nanowires, where the logarithm of nanowire (NW) number is plotted with respect to misalignment angle. **e.** Histograms of relative resistance (resistance/average resistance). Data were collected from 40 sensors based on 2D nanowire arrays (orange), 3D nanoarchitecture (red), drop-casted nanowires (blue) and screen-printed nanoparticles (green).

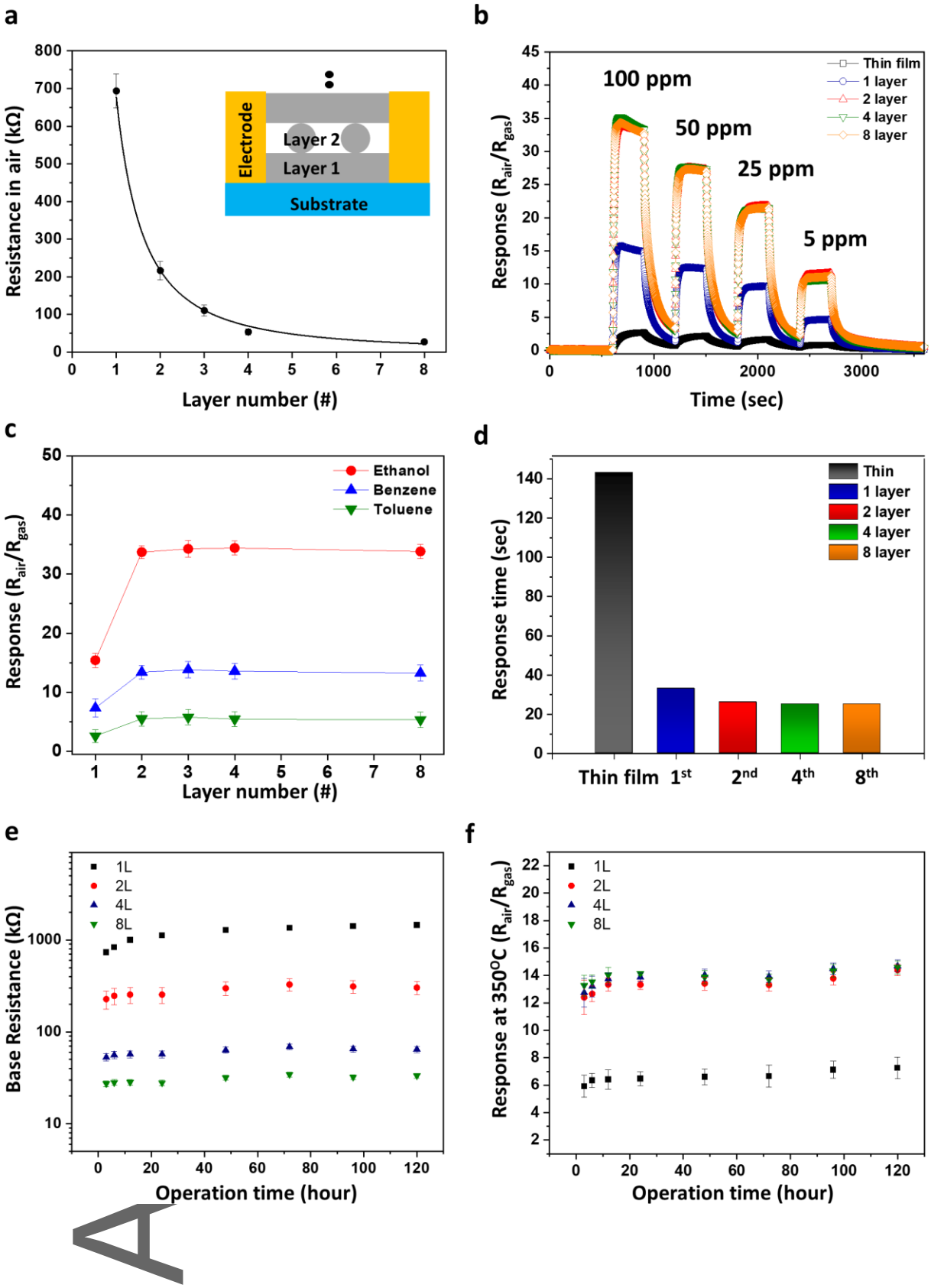

Figure 2. 3D nanostructure engineering to investigate its impact on sensor performance. a. Dependence of resistance in air on stacking layer number. **b.** Dynamic ethanol gas response comparing thin film vs 1, 2, 4 and 8 layer devices in concentration range of 5 – 100 ppm at 350^{O}C. **c.** Sensor response dependence for 100 ppm of ethanol (red), benzene (blue) and toluene (green) at 350^{O}C as function of layer number. **d.** Response time for 100 ppm of ethanol gas at 350^{O}C. (**e-f**) Stability test results. Changes of **e.** baseline resistance and **f.** response as a function of operation time.

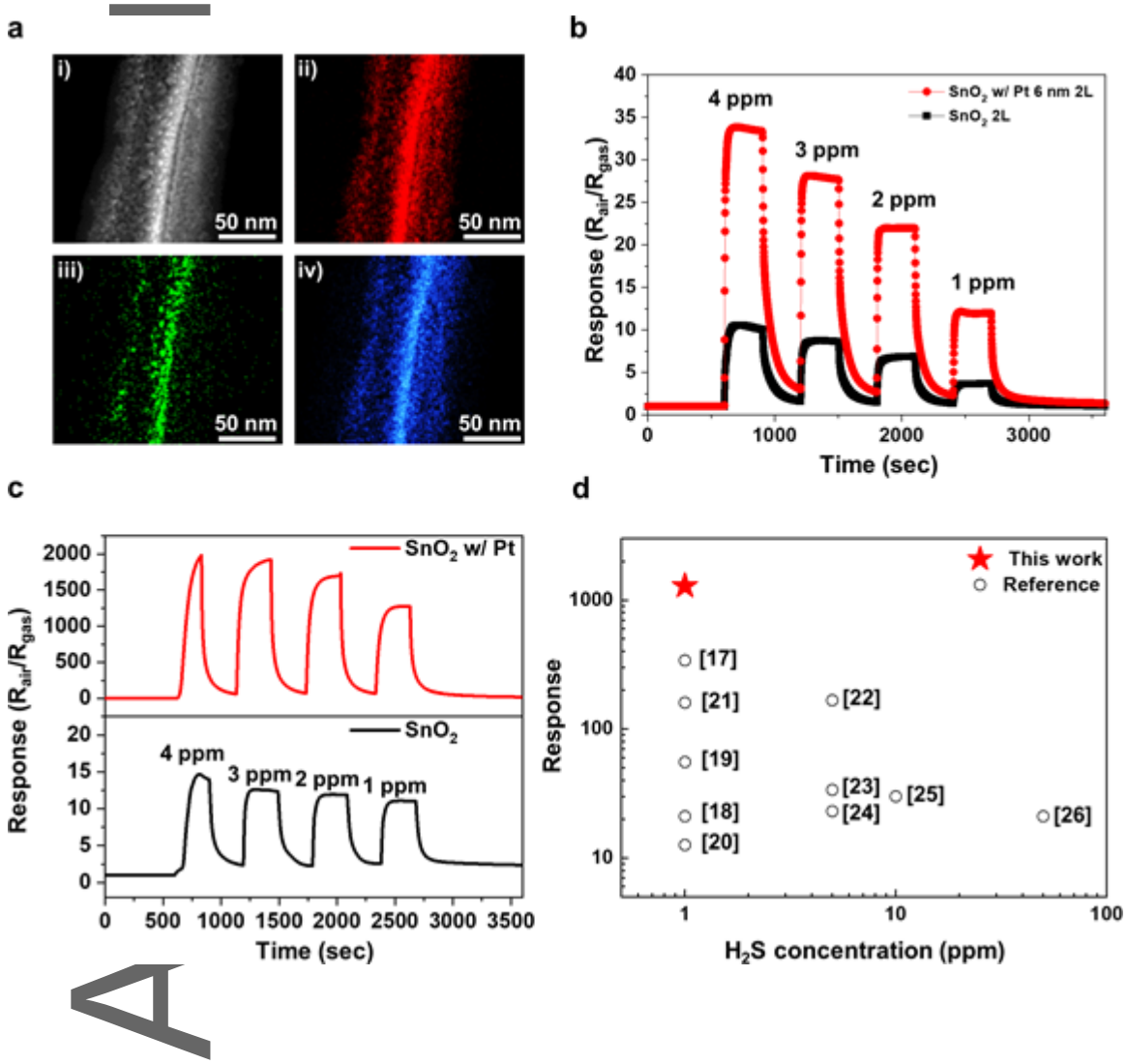

Figure 3. Gas-sensing performance of 3D-stacked SnO_2 nanowires decorated with Pt. a. i) High-angle annular dark-field scanning TEM image of Pt-decorated SnO_2 nanowire and EDX mapping of ii) Sn, iii) Pt and iv) O on the surface of nanowires. **b.** Response to ethanol vapor at 350^{O}C of 2 layer stacked SnO_2 and Pt (6 nm) decorated SnO_2. **c.** H_2S sensing response at 300 °C, in concentration range of 1–4 ppm, of the Pt/ SnO_2 and SnO_2 nanowires. **d.** Comparison of gas response (R_{air}/R_{gas} or R_{gas}/R_{air}) of MOS based sensor toward H_2S in this work to those reported in the literature since 2000.

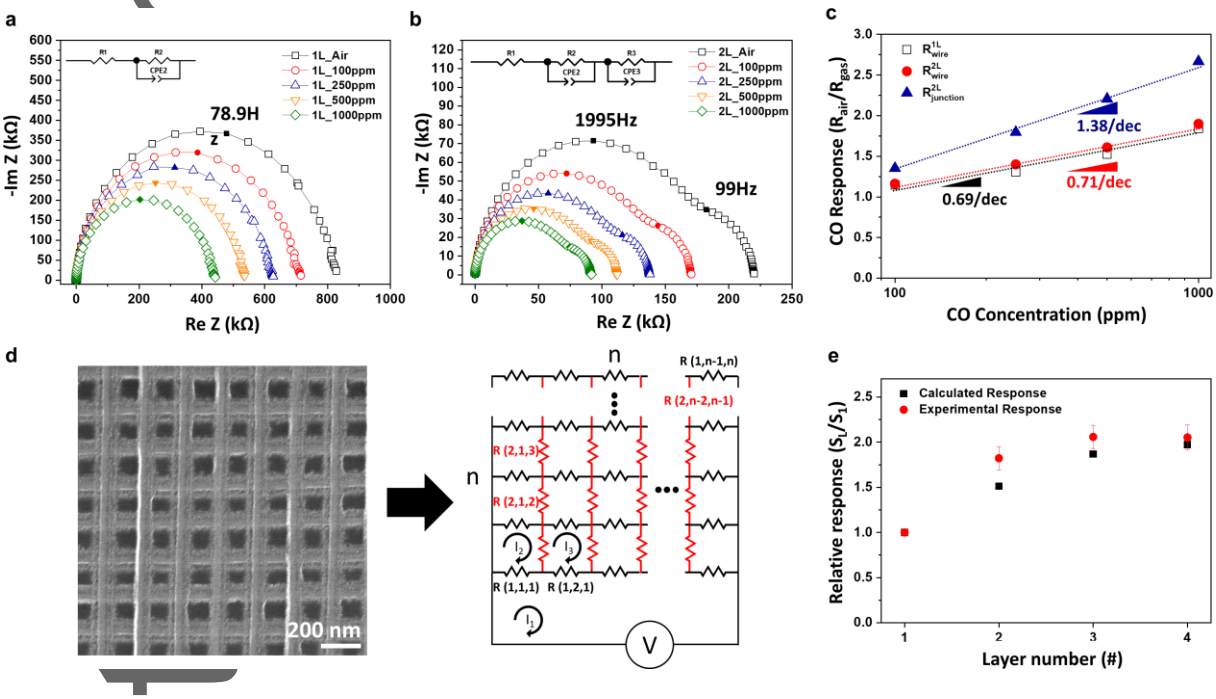

Figure 4. Sensitivity of impedance and equivalent circuit elements to changes in atmosphere. Nyquist plots of impedance data were obtained for several different nanostructures following

exposure to CO in the concentration range of 100–1000 ppm at 350^{O}C. **a.** 2D nanowire arrays, **b.** Stacked structures (2 layers). **c.** Response dependence of the different indicated electrical components on CO concentration in the range of 100–1000 ppm at 350^{O}C. **d.** SEM image of 2 layer stacked 3D crossed-wire SnO_2 nanostructure and schematic image of resistor network with n x n structure. **e.** Relative response (S_l/S_1) dependence on layer number - experimental (red) vs calculated response (black).

Simple downsizing of nano-building blocks and their assembly typically exhibits a large device-to-device variation in gas sensor performance due to unpredictable electrical conduction pathways. This study demonstrates that systemically controlled 3-dimensional (3D) nanostructures can achieve both high sensing response and reproducibility. Combining electrical characterization with equivalent circuit modeling provides important insights into the electrical conduction in 3D assemblies and their gas-sensing mechanism.